Myofibroblasts acquire retinoic acid–producing ability during fibroblast-to-myofibroblast transition following kidney injury

OPEN

Jin Nakamura[1,7,8], Yuki Sato[1,2,8], Yuichiro Kitai[1,8], Shuichi Wajima[1,3], Shinya Yamamoto[1], Akiko Oguchi[1], Ryo Yamada[1,9], Keiichi Kaneko[1], Makiko Kondo[1], Eiichiro Uchino[1], Junichi Tsuchida[2,4,10], Keita Hirano[1], Kumar Sharma[5], Kenji Kohno[6] and Motoko Yanagita[1]

[1]Department of Nephrology, Kyoto University Graduate School of Medicine, Kyoto, Japan; [2]TMK Project, Kyoto University Graduate School of Medicine, Kyoto, Japan; [3]Nephrology Research Laboratories, Nephrology R&D Unit, R&D Division, Kyowa Hakko Kirin; [4]Research Unit/Nephrological & Endocrinological Science, Sohyaku, Innovative Research Division, Mitsubishi Tanabe Pharma Corporation, Saitama, Japan; [5]Center for Renal Precision Medicine, Division of Nephrology, Department of Medicine, University of Texas Health San Antonio; and [6]Graduate School of Biological Sciences, Institute for Research Initiatives, Nara Institute of Science and Technology, Nara, Japan

Tubular injury and interstitial fibrosis are the hallmarks of chronic kidney disease. While recent studies have verified that proximal tubular injury triggers interstitial fibrosis, the impact of fibrosis on tubular injury and regeneration remains poorly understood. We generated a novel mouse model expressing diphtheria toxin receptor on renal fibroblasts to allow for the selective disruption of renal fibroblast function. Administration of diphtheria toxin induced upregulation of the tubular injury marker Ngal and caused tubular proliferation in healthy kidneys, whereas administration of diphtheria toxin attenuated tubular regeneration in fibrotic kidneys. Microarray analysis revealed down-regulation of the retinol biosynthesis pathway in diphtheria toxin-treated kidneys. Healthy proximal tubules expressed retinaldehyde dehydrogenase 2 (RALDH2), a rate-limiting enzyme in retinoic acid biosynthesis. After injury, proximal tubules lost RALDH2 expression, whereas renal fibroblasts acquired strong expression of RALDH2 during the transition to myofibroblasts in several models of kidney injury. The retinoic acid receptor (RAR) RARγ was expressed in proximal tubules both with and without injury, and αB-crystallin, the product of an RAR target gene, was strongly expressed in proximal tubules after injury. Furthermore, BMS493, an inverse agonist of RARs, significantly attenuated tubular proliferation in vitro. In human biopsy tissue from patients with IgA nephropathy, detection of RALDH2 in the interstitium correlated with older age and lower kidney function. These results suggest a role of retinoic acid signaling and cross-talk between fibroblasts and tubular epithelial cells during tubular injury and regeneration, and may suggest a beneficial effect of fibrosis in the early response to injury.

Kidney International (2019) ■, ■–■; https://doi.org/10.1016/j.kint.2018.10.017

KEYWORDS: chronic kidney disease; fibroblast; fibrosis; proximal tubule

Renal fibrosis and tubular injury are the hallmarks of chronic kidney disease and predict its prognosis. Renal fibrosis is mediated by the accumulation of myofibroblasts,[1] whose major origins have been identified as resident fibroblasts and pericytes.[2–6] Because renal fibroblasts are in close contact with tubular epithelial cells, cross talk between these 2 cell types has been proposed. We and another group have generated proximal tubule–specific injury models using proximal tubule–specific Cre strains[7] and demonstrated that proximal tubule injury triggers the activation of fibroblasts and pericytes, leading to fibrosis.[8,9]

Although the role of proximal tubule injury in the progression of fibrosis is well accepted, few studies have clarified the pathologic relevance of fibrosis in the progression of chronic kidney disease. Because the extent of interstitial fibrosis correlates well with renal prognosis, fibrosis has been considered as a self-sustained deteriorating process that injures the adjacent nephrons. On the other hand, some investigators have argued the possibility that fibrosis might have a beneficial impact. Fujigaki *et al.*[10] observed the emergence of myofibroblasts around injured tubules in an acute kidney injury model and postulated that fibrosis might function as a structural support for damaged nephrons during regeneration. Kaissling *et al.*[11] also proposed the concept that fibrosis itself is not deteriorating but might support tubular recovery.

Correspondence: *Motoko Yanagita, Department of Nephrology, Kyoto University Graduate School of Medicine, Shogoin-Kawahara-cho 54, Sakyo-ku, Kyoto 606-8507, Japan. E-mail: motoy@kuhp.kyoto-u.ac.jp*

[7]The present address of JN is Candidate Discovery Laboratories Unit 1, Drug Discovery Research, Astellas Pharma Inc., Ibaraki, Japan.

[8]JN, YS, and YK contributed equally to this work.

[9]The present address of RY is Shizuoka General Hospital, Shizuoka, Japan.

[10]The present address of JT is Research Unit/Innovative Medical Science, Sohyaku, Innovative Research Division, Mitsubishi Tanabe Pharma Corporation, Saitama, Japan.

Received 9 January 2018; revised 25 September 2018; accepted 4 October 2018

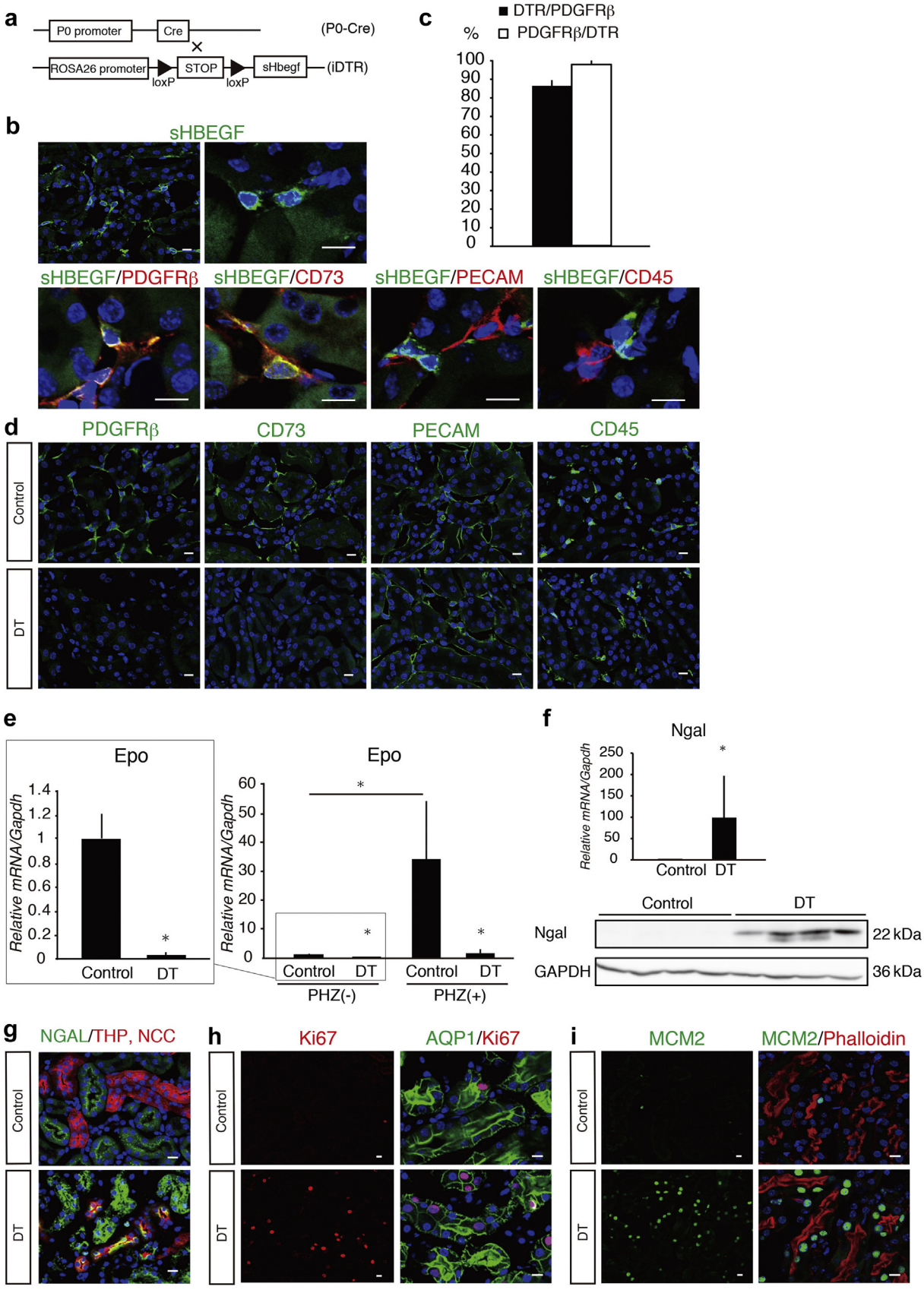
a
P0 promoter
Cre
(P0-Cre)
ROSA26 promoter
STOP
sHbegf
(iDTR)
loxP
loxP
b
sHBEGF
sHBEGF/PDGFRβ
sHBEGF/CD73
sHBEGF/PECAM
sHBEGF/CD45
c
DTR/PDGFRβ
PDGFRβ/DTR
%
d
PDGFRβ
CD73
PECAM
CD45
Control
DT
e
Epo
Relative mRNA/Gapdh
Control
DT
PHZ(-)
PHZ(+)
f
Ngal
Relative mRNA/Gapdh
Control
DT
GAPDH
22 kDa
36 kDa
g
NGAL/THP, NCC
h
Ki67
AQP1/Ki67
i
MCM2
MCM2/Phalloidin

Whether fibrosis is deteriorating in its nature or could be beneficial in some contexts is an essential question from the standpoint of therapeutic application, yet the lack of compounds capable of reversing fibrosis hinders the analysis necessary to answer it.

Here, we established a novel model of fibroblast dysfunction and proposed possible beneficial roles of fibroblasts and myofibroblasts in healthy and diseased kidneys. We further demonstrated that fibroblasts acquire retinoic acid (RA)–producing capacity during the transition to myofibroblasts, which possesses the capacity to promote the regeneration of proximal tubules.

RESULTS

Fibroblast-specific expression of diphtheria toxin receptor in the kidneys of *P0-Cre:iDTR* mice

Previously, we have shown that resident fibroblasts in the cortex and outer medulla of the kidney are lineage labeled with *P0-Cre* transgenic mice[12] and that they transdifferentiate into myofibroblasts during kidney injury.[2] To halt protein synthesis specifically in renal fibroblasts, we crossed *P0-Cre* mice with i–diphtheria toxin receptor (DTR) mice[13,14] in which Cre recombinase excises the STOP cassette and induces the expression of DTR, also known as simian heparin-binding epidermal growth factor–like growth factor (sHbegf) (Figure 1a). DTR was effectively and specifically expressed in the platelet–derived growth factor receptor (PDGFR)-β^+ fibroblasts in the interstitium of the cortex and outer medulla but not in endothelial cells or hematopoietic cells (Figure 1b and c). DTR$^+$ cells in the cortex also expressed CD73, a cortical fibroblast marker (Figure 1b).

Loss of fibroblast markers in the interstitium after diphtheria toxin administration

Diphtheria toxin (DT) binds to its receptor on the cell surface, is incorporated via endocytosis, and halts protein synthesis in the target cell.[13,15] We injected *P0-Cre:iDTR* mice with 25 ng/g DT i.p. and humanely killed them 3 days after the administration. Although histologic analysis did not show any abnormalities except for sporadic vacuolation in proximal tubules (Supplementary Figure S1A), immunostaining revealed the ablation of PDGFR-β and CD73 expression but not of CD45 or platelet endothelial cell adhesion molecule (PECAM) expression, indicating the fibroblast-specific cessation of protein synthesis or the loss of fibroblasts (Figure 1d). We estimated the number of fibroblasts in the interstitium by staining hematopoietic cells and endothelial cells before and after DT administration and found that some of the fibroblasts survive and reside in the interstitium after DT administration, although the number of fibroblasts decreased to some extent (Supplementary Figure S1B). Interestingly, the numbers of hematopoietic cells and endothelial cells were not significantly changed after DT treatment, which excludes the possibility of severe inflammation or capillary loss after DT treatment.

Significant reduction of erythropoietin production after DT administration

Previously we demonstrated that most erythropoietin (Epo)-producing cells were lineage labeled with *P0-Cre*,[2] but the contribution of other populations to Epo production remains unclear. The expression of *Epo* mRNA was completely abolished in the kidneys of *P0-Cre:iDTR* mice after the administration of DT (Figure 1e) and was not increased even in the presence of severe hemolytic anemia induced by the administration of phenylhydrazine (Figure 1e), supporting our previous conclusion that *P0-Cre* lineage-labeled fibroblasts predominantly contribute to Epo production.[2]

DT administration induces upregulation of neutrophil gelatinase–associated lipocalin and tubular proliferation

Next, we focused on the phenotypic changes of tubular epithelial cells in this system. Although DT administration did not cause massive apoptosis in proximal tubules (Supplementary Figure S1C), DT administration causes upregulation of neutrophil gelatinase–associated lipocalin (Ngal) mRNA and protein (Figure 1f and g). Significant proliferation of proximal tubules shown by the immunostaining of Ki67 (Figure 1h) and MCM2 (Figure 1i) also was observed in the corticomedullary junction after DT administration. We also confirmed that the administration of DT to *P0-Cre* mice (without DTR) did not induce the upregulation of Ngal, histologic injury, or renal dysfunction,

Figure 1 | Diphtheria toxin (DT) administration to *P0-Cre:iDTR* mice abolishes erythropoietin (Epo) production, increases neutrophil gelatinase–associated lipocalin (Ngal) expression, and induces tubular proliferation. (**a**) Schematic demonstration of *P0-Cre* mice and *iDTR* mice. (**b**) Immunostaining of simian heparin-binding epidermal growth factor–like growth factor (sHBEGF; diphtheria toxin receptor: DTR) in the kidney. sHBEGF was co-localized with platelet–derived growth factor receptor (PDGFR-β; a fibroblast marker) and CD73 (a cortical fibroblast marker), but not with platelet endothelial cell adhesion molecule (PECAM; an endothelial marker) and CD45 (a leucocyte marker). (**c**) Graph illustrating the proportion of PDGFRβ$^+$ interstitial cells expressing sHBEGF (%DTR/PDGFR-β) and the proportion of DTR$^+$ interstitial cells expressing PDGFR-β (%PDGFR-β/DTR). DTR was effectively and specifically expressed in the PDGFR-β$^+$ fibroblasts ($n = 4$). (**d**) Immunostaining of PDGFR-β, CD73, PECAM, and CD45 before and after DT administration. DT administration ablated the expression of PDGFR-β and CD73 but not CD45 or PECAM. (**e**) Real-time reverse transcriptase–polymerase chain reaction (RT-PCR) analysis showed significant reduction of *Epo* mRNA after DT administration even in the presence of severe anemia caused by phenylhydrazine (PHZ) administration ($n = 4$–5). $F = 18.26$, $P < 0.05$ for interaction; $F = 20.56$, $P < 0.05$ for DT; $F = 21.57$, $P < 0.05$ for PHZ. F and P values are from 2-way analysis of variance after Bonferroni's *post hoc* test. *$P < 0.05$. (**f**) Real-time RT-PCR and Western blot analysis revealed the strong induction of *Ngal* mRNA and protein after DT administration, indicating the presence of tubular injury ($n = 6$–8). Statistical analysis by Student *t*-test. *$P < 0.05$. (**g**) Immunostaining revealed the induction of Ngal in Tamm Horsfall protein (THP)- or Na-Cl cotransporter (NCC)–positive distal tubules after DT administration, indicating the presence of tubular injury. (**h,i**) Immunostaining of Ki67 (**h**) and MCM2 (**i**) showed the proliferation of proximal tubules in the corticomedullary junction after DT administration. GADPH, glyceraldehyde-3-phosphate dehydrogenase. Bars = 10 μm. To optimize viewing of this image, please see the online version of this article at www.kidney-international.org.

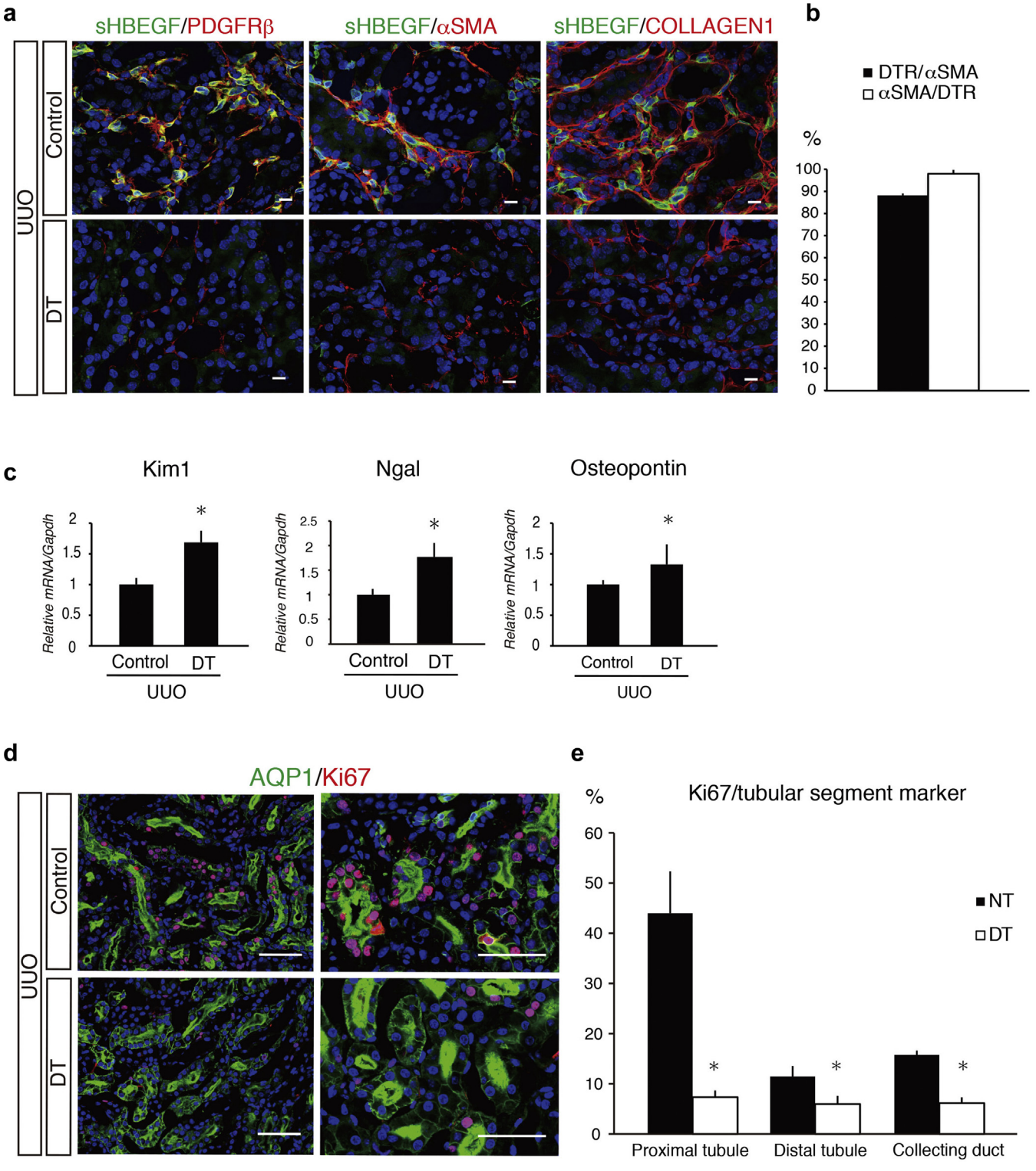

Figure 2 | Diphtheria toxin (DT) administration increases tubular injury markers and attenuates tubular regeneration in fibrotic kidney. (**a**) Immunostaining revealed the co-localization of simian heparin-binding epidermal growth factor–like growth factor (sHBEGF) with platelet–derived growth factor receptor (PDGFR-β), α-SMA (a marker for myofibroblast), and Collagen 1 in unilateral ureteral obstruction (UUO) kidneys of *P0-Cre:iDTR* mice and the ablation of these expressions after DT administration. (**b**) Graphs illustrate that most αSMA^{+} interstitial cells co-expressed sHBEGF (%sHBEGF/αSMA) and that most sHBEGF^{+} interstitial cells co-expressed α-SMA (%α-SMA/hHBEGF), indicating the effective and specific expression of diphtheria toxin receptor (DTR) in myofibroblasts ($n = 4$). (**c**) Real-time reverse transcriptase–polymerase chain reaction analysis revealed significant upregulation of *Kim1*, neutrophil gelatinase–associated lipocalin *(Ngal),* and *Osteopontin* ($n = 5$). Statistical analysis by Student *t*-test. *$P < 0.05$. (**d**) Immunostaining of Ki67 and AQP1 (a marker of proximal tubules). Numbers of Ki67^{+} proximal tubules significantly decreased after DT administration. (**e**) Graph illustrating the proportion of Ki67^{+} cells co-expressing AQP1 (continued)

which excludes the possibility of the direct toxicity of DT (Supplementary Figure S2A).

DT administration increases tubular injury markers and attenuates tubular proliferation in fibrotic kidney

We next investigated the role of myofibroblasts in the unilateral ureteral obstruction (UUO) model using the same system.

DTR$^+$ cells in UUO kidney of *P0-Cre:iDTR* mice were positive for PDGFR-β, α-SMA, and collagen 1 (Figure 2a, upper panel). DTR was effectively and specifically expressed in myofibroblasts (Figure 2b). The administration of DT to *P0-Cre:iDTR* mice with UUO significantly decreased the expression of DTR, PDGFR-β, α-SMA, and collagen 1 (Figure 2a, lower panel). These results support our previous findings that most myofibroblasts are linage labeled with *P0-Cre* and are transdifferentiated from resident fibroblasts.[2]

Although histologic change was not obvious in periodic acid–Schiff staining (Supplementary Figure S1A), the expression levels of *Kim1, Ngal,* and *osteopontin* mRNA were significantly increased in UUO kidneys after DT administration (Figure 2c).

We also examined the effect of DT administration on tubular proliferation. Whereas Ki67 staining was abundantly detected in tubular epithelial cells in UUO kidneys, the number of Ki67-positive cells was significantly decreased after the administration of DT (Figure 2d), and this decrease was most prominent in the proximal tubules (Figure 2e, Supplementary Figure S2B). Because tubular proliferation is essential for tubular regeneration, reduction of tubular proliferation possibly attenuates tubular regeneration.

Dysregulation of RA signaling pathway in DT-treated kidney

To explore how DT administration to the mice expressing DTR in fibroblasts affects tubular maintenance, we performed microarray analysis with use of the kidneys of *P0-Cre:iDTR* mice with or without DT administration. We selected the transcripts that were upregulated or downregulated more than 2-fold (2329; Supplementary Table S1), as well as those that were expressed more than 5 times higher in the kidneys than in other tissues (1311); pairwise comparisons of these groups revealed 275 transcripts common to each group (Figure 3a).

These transcripts were uploaded to Ingenuity Pathways Analysis, which identified the dysregulation of genes involved in retinol biosynthesis as the most statistically significant. Additionally, the software identified the dysregulation of genes involved in stearate biosynthesis, leucine degradation, mineralocorticoid biosynthesis, and serotonin receptor signaling (Table 1).

Whereas RA signaling is essential in prenatal kidney development, the role of RA signaling after birth remains unclear.[16] Dietary carotenoid and retinyl ester are absorbed in the intestine and converted into retinol, which binds to retinol binding protein 4 (RBP4) and transthyretin (TTR). The retinol-RBP-TTR complex is taken up by the target cells through an RBP receptor called "stimulated by RA 6" (STRA6; Figure 3b).[17,18] After entering the target cells, retinol binds to RBP1, a cellular retinol binding protein, and is either esterified to be stored in the cells[19] or oxidized into retinal. Retinal is finally converted to RA by retinaldehyde dehydrogenase (Figure 3b)[20,21] and then can bind to nuclear receptors including RARs and RXRs. The role of RA signaling and the expression of its key molecules have been extensively analyzed in the liver but not in the kidney.

Immunostaining demonstrated that STRA6 was expressed exclusively in the basolateral sides of the proximal tubules in healthy kidneys, indicating the possible uptake of retinol from peritubular capillaries. STRA6 expression in the proximal tubules was downregulated after DT administration (Figure 3c) as confirmed by Western blotting in UUO kidneys (Figure 3d).

Relocation of RA-producing capacity from proximal tubules to myofibroblasts

Among the retinaldehyde dehydrogenases (RALDHs), RALDH-1, -2, and -3 convert retinal to RA, and the relative contributions of these enzymes differ between cells and tissues.[22] GeneChip analysis in the Gene Expression Omnibus (GEO) database comparing healthy and UUO kidneys[23] showed that *RALDH2* expression was significantly upregulated in UUO kidneys (Supplementary Figure S3A), whereas *RALDH1* expression was comparable between healthy and UUO kidneys. *RALDH3* was almost absent in both healthy and UUO kidneys.

We also found that the expression of *RALDH2* mRNA and protein was significantly upregulated in UUO kidneys of *P0-Cre:iDTR* mice (Figure 3d and e), whereas the expression of *RALDH1* mRNA was comparable between healthy and UUO kidneys (Supplementary Figure S3B). In immunostaining, RALDH1 expression was observed in tubular epithelial cells in both healthy and UUO kidneys (Supplementary Figure S3C). On the contrary, the faint expression of RALDH2 in the proximal tubules of healthy kidneys vanished after UUO (Figure 3c). Alternatively, strong RALDH2 expression was seen in the interstitium of UUO kidneys and was co-localized with PDGFR-β and α-SMA (Figure 3c and f) but was abolished by the administration of DT (Figure 3c) as confirmed by real-time reverse transcriptase–polymerase chain reaction analysis and Western blotting (Figure 3d and e). We also sorted fibroblasts and myofibroblasts from healthy and fibrotic kidneys utilizing *P0-Cre:R26tdTomato* mice and

Figure 2 | (continued) (a marker of proximal tubules), Tamm Horsfall protein, or Na-Cl cotransporter (markers of distal tubules) and AQP2 (a marker of collecting ducts) in each segment before and after DT administration ($n = 4$). $F = 31.63$, $P < 0.05$ for interaction; $F = 98.80$, $P < 0.05$ for DT; $F = 37.48$, $P < 0.05$ for tubular segment. *F* and *P* values are from 2-way analysis of variance after Bonferroni's *post hoc* test. NT, nontreated. *$P < 0.05$. Bars = 10 μm (**a**), 50 μm (**d**). To optimize viewing of this image, please see the online version of this article at www.kidney-international.org.

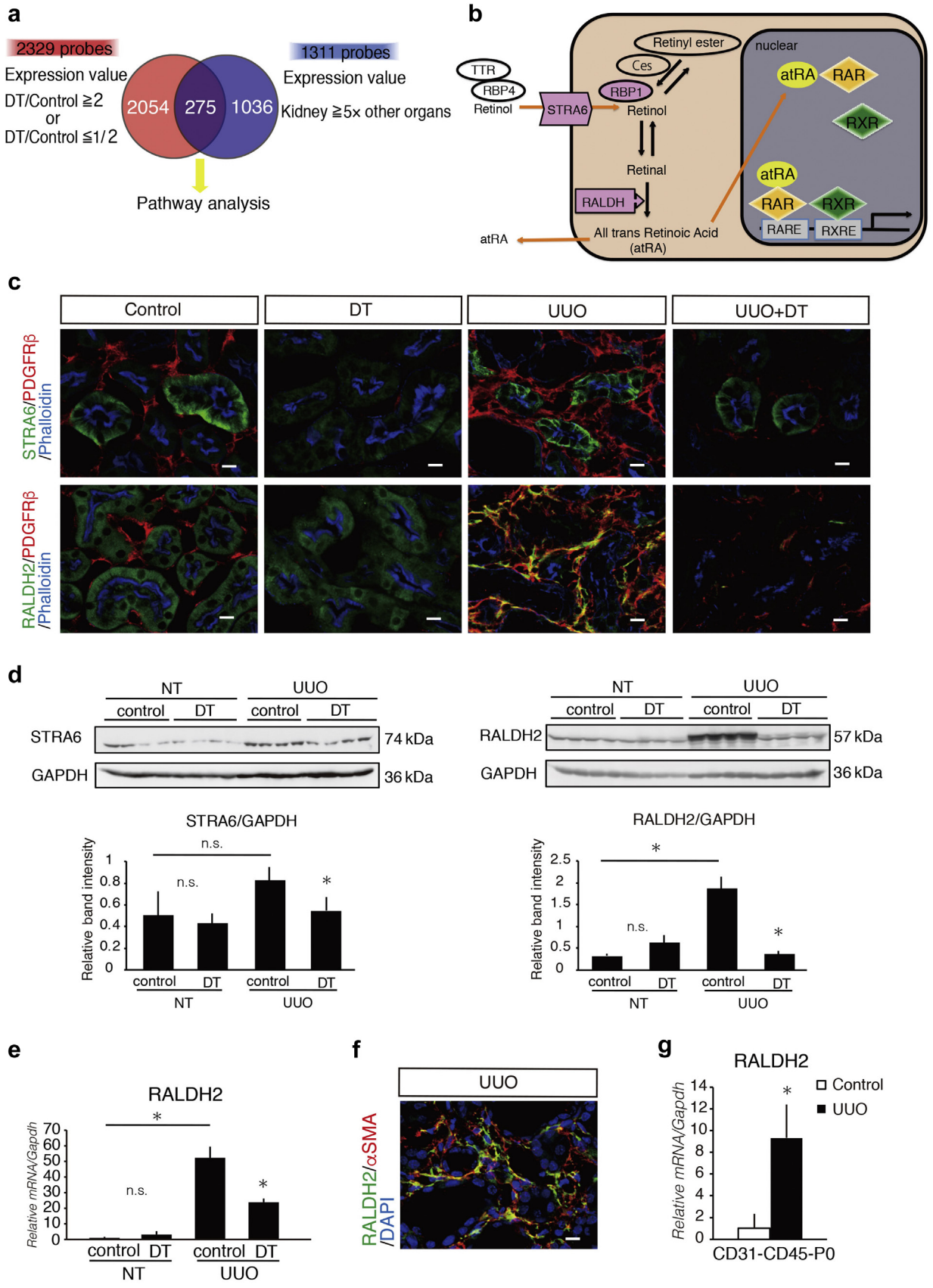
a
2329 probes
Expression value
DT/Control ≧2
or
DT/Control ≦1/2
2054
275
1036
1311 probes
Expression value
Kidney ≧5× other organs
Pathway analysis
b
TTR
RBP4
Retinol
STRA6
Retinyl ester
Ces
RBP1
Retinol
Retinal
RALDH
All trans Retinoic Acid (atRA)
atRA
nuclear
atRA
RAR
RXR
atRA
RAR
RXR
RARE
RXRE
c
Control
DT
UUO
UUO+DT
STRA6/PDGFRβ /Phalloidin
RALDH2/PDGFRβ /Phalloidin
d
NT
UUO
control
DT
STRA6
74 kDa
GAPDH
36 kDa
RALDH2
57 kDa
STRA6/GAPDH
Relative band intensity
n.s.
*
RALDH2/GAPDH
e
RALDH2
Relative mRNA/Gapdh
f
UUO
RALDH2/αSMA /DAPI
g
RALDH2
Control
UUO
Relative mRNA/Gapdh
CD31-CD45-P0

Table 1 | Top 5 signaling pathways identified by Ingenuity Pathways Analysis

Ingenuity Canonical Pathways	-log (*P* value)	Ratio	Molecules
Retinol biosynthesis	3.55	8.2E-02	Ces1e,AADAC,RDH10,Ces1d,Ces2b/Ces2c
Stearate biosynthesis I (animals)	3.14	8E-02	Ces1e,DHCR24,Acot1,ACSL1
Leucine degradation I	2.35	7.69E-02	BCAT1,IVD
Mineralocorticoid biosynthesis	2.26	9.52E-02	HSD3B2,Hsd3b4 (includes others)
Serotonin receptor signaling	2.2	6.52E-02	DDC,SLC18A1,PCBD1

verified the induction of *RALDH2* mRNA in myofibroblasts (Figure 3g).

Taken together, the evidence suggests that myofibroblasts acquire strong expression of RALDH2 during the transition from fibroblasts, whereas proximal tubules lose their RALDH2 expression upon injury. A previous study that analyzed the transcriptional profiles of medullary myofibroblasts using translational ribosome affinity purification identified the *RALDH2* gene as one of the genes upregulated in myofibroblasts.[24]

Reversible acquisition of RA-producing ability by myofibroblasts in various types of kidney disease models. Next we analyzed the expression profile of RALDH2 in other kidney disease models with tubular injury and interstitial fibrosis, namely, an adenine nephropathy (AN) model and a severe ischemic reperfusion injury (IRI) model induced by 45-minute ischemia (Figure 4a).

Similar to the results seen in the UUO model, the faint RALDH2 expression in the proximal tubules disappeared in diseased kidneys, whereas a strong expression emerged in myofibroblasts as observed in the UUO model (Figure 4a). The upregulation of RALDH2 mRNA and protein also was confirmed by real-time reverse transcriptase–polymerase chain reaction analysis and Western blotting (Figure 4b).

We also examined whether the relocation of RALDH2 expression from the proximal tubules to the myofibroblasts is reversible utilizing 3 types of reversible kidney disease models, reversible UUO (rUUO), reversible moderate IRI, and reversible AN (Supplementary Figure S4). In these models, the strong expression of RALDH2 in myofibroblasts disappeared after kidney regeneration (Figure 4c) as confirmed by real-time reverse transcriptase–polymerase chain reaction analysis (Figure 4d).

Expression of RAR-γ in proximal tubules but not in fibroblasts. In adult kidneys, RA agonists reduce tubular injury and attenuate fibrosis in various kidney injury models.[25–29] To explore the RA action site, we analyzed the localization of the RA receptor (RAR) family and found that RAR-γ was expressed in proximal tubules (Figure 5). The expression of RA receptors in the interstitium, however, was sparse even in injured kidneys, suggesting that RA might primarily act on proximal tubules and induce their regeneration by its binding to RAR-γ.

Possible function of RA signaling in proximal tubules

We further analyzed the possible function of RA signaling in tubular epithelial cells and found that the administration of BMS493, an inverse agonist of pan-retinoic acid receptors, to NRK52E cells, a tubule cell line, attenuated tubular cell proliferation (Figure 6a). In addition, the expression of *Ki67* mRNA, total cell number, and BrdU incorporation were lower in the presence of BMS493 (Figure 6b and c). These results indicate the importance of RA in tubular cell proliferation. We also explored RA downstream signaling in injured kidneys and found that in healthy kidneys, αB-crystallin, the product of an RAR target gene,[30] was expressed only sparsely in the S3 segment of proximal tubules, parietal epithelial cells of glomeruli, and medullary epithelial cells (Figure 6d) but was strongly upregulated only in proximal tubules in injured kidneys (Figure 6e and f).

Figure 3 | Dysregulation of retinoic acid (RA) signaling pathway in diphtheria toxin (DT)–treated kidney. (**a**) We identified 2329 differentially expressed transcripts (red) that showed at least a 2-fold change in gene expression in *P0-Cre:iDTR* kidneys compared with control subjects, and 1311 transcripts (blue) that showed expression levels at least 5 times higher in the kidneys than in other tissues. Pathway analysis was performed on the 275 transcripts that were in both groups. (**b**) Schematic drawing of RA metabolism. (**c**) Immunostaining of key molecules in RA metabolism (stimulated by RA 6 [STRA6], retinaldehyde dehydrogenase [RALDH]2) in normal kidney (control) and unilateral ureteral obstruction (UUO) kidney with or without DT administration. (**d**) Western blot analysis and the quantification of the bands showed that STRA6 expression in UUO kidneys was decreased after DT administration ($n = 4$). $F = 1.96$, $P = 0.1867$ for interaction; $F = 9.11$, $P < 0.05$ for UUO; $F = 5.86$, $P < 0.05$ for DT. Western blot analysis and quantification of the bands also showed that RALDH2 expression was significantly increased in UUO kidneys but was decreased after DT administration ($n = 4$). $F = 83.41$, $P < 0.05$ for interaction; $F = 42.33$, $P < 0.05$ for UUO; $F = 37.21$, $P < 0.05$ for DT. *F* and *P* values are from 2-way analysis of variance (ANOVA) after Bonferroni's *post hoc* test. $^*P < 0.05$. (**e**) Real-time reverse transcriptase–polymerase chain reaction (RT-PCR) analysis revealed that the expression levels of *RALDH2* were increased in UUO kidneys but were significantly decreased after DT administration (n = 5-8). $F = 91.49$, $P < 0.05$ for interaction; $F = 67.84$, $P < 0.05$ for UUO; $F = 507.64$, $P < 0.05$ for DT. *F* and *P* values are from 2-way ANOVA after Bonferroni's *post hoc* test. $^*P < 0.05$. (**f**) RALDH2-positive interstitial cells were also positive for α-SMA (a marker of myofibroblasts). (**g**) Real-time RT-PCR analysis revealed significant induction of *RALDH2* expression in $CD31^-CD45^-Tomato^+$ cells (CD31-CD45-P0) isolated from *P0-Cre:R26tdTomato* mice in UUO kidneys ($n = 3$). Statistical analysis by Student *t*-test. $^*P < 0.05$. Bars = 20 μm. Ces, carboxylesterase; n.s., not significant; DAPI, 4′,6-diamidino-2-phenylindole; GADPH, glyceraldehyde-3-phosphate dehydrogenase; PDGFR, platelet–derived growth factor receptor; RAR, retinoic acid receptor; RARE, retinoic acid response element; RBP1, retinol binding protein 1; RBP4: retinol binding protein 4; RXR, retinoid X receptor; RXRE, retinoid X response element; TTR, transthyretin. To optimize viewing of this image, please see the online version of this article at www.kidney-international.org.

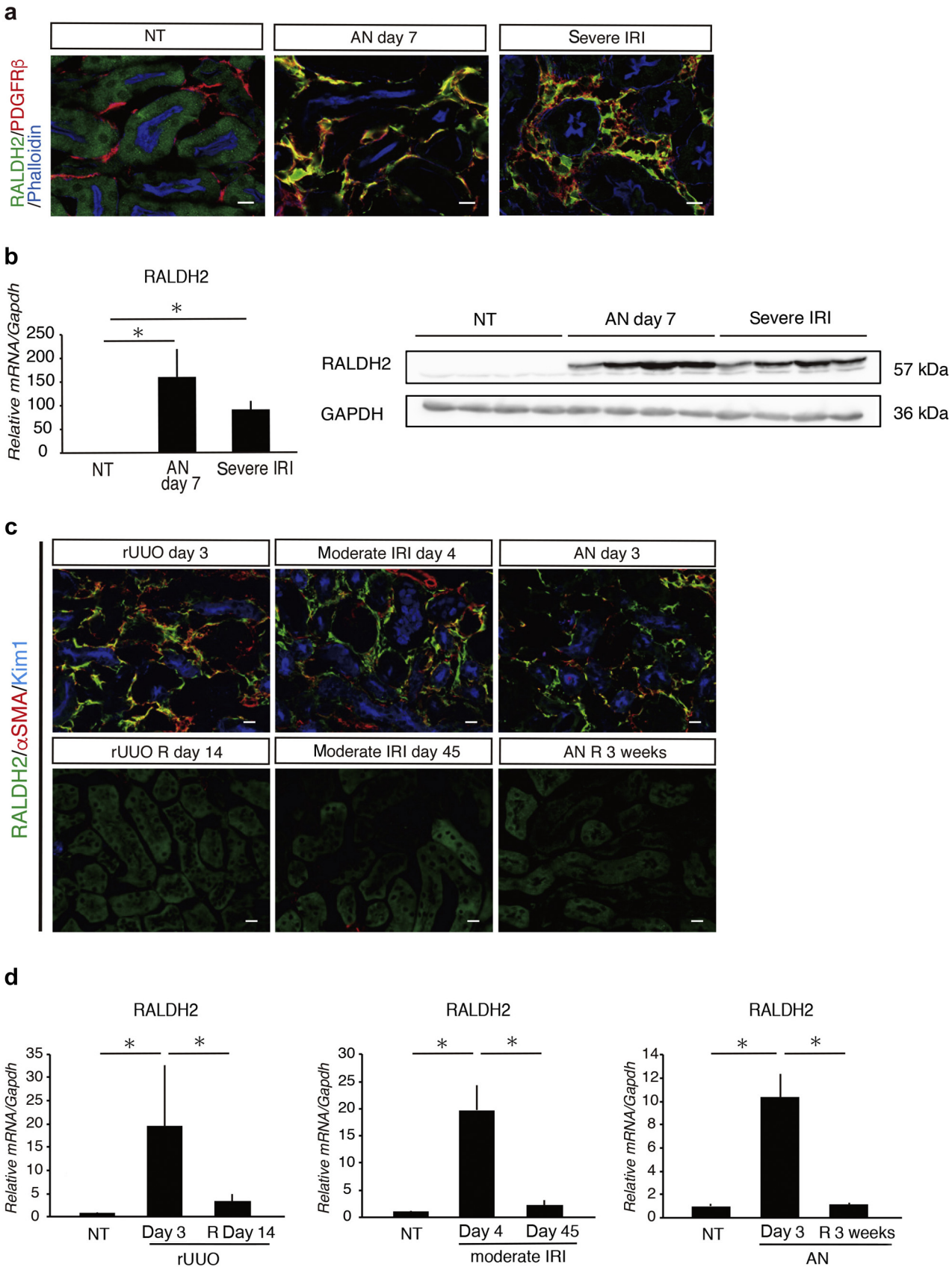
a
NT
AN day 7
Severe IRI
RALDH2/PDGFRβ
/Phalloidin
b
RALDH2
Relative mRNA/Gapdh
250
200
150
100
50
0
NT
AN day 7
Severe IRI
NT
AN day 7
Severe IRI
RALDH2
57 kDa
GAPDH
36 kDa
c
rUUO day 3
Moderate IRI day 4
AN day 3
rUUO R day 14
Moderate IRI day 45
AN R 3 weeks
RALDH2/αSMA/Kim1
d
RALDH2
Relative mRNA/Gapdh
NT
Day 3
R Day 14
rUUO
RALDH2
NT
Day 4
Day 45
moderate IRI
RALDH2
NT
Day 3
R 3 weeks
AN

Acquisition of RALDH2 expression by myofibroblasts in human kidney disease

RALDH2 expression also was analyzed in kidney biopsy samples of patients with IgA nephropathy. Whereas RALDH2 was strongly expressed in healthy tubular epithelial cells (Figure 7a, left), it also was detected in the interstitium of some biopsy samples (Figure 7a, right). Patients with positive RALDH2 staining in the interstitium were significantly older and had lower kidney function (Figure 7b). Other characteristics including sex and risk factors such as hypertension, diabetes mellitus, and dyslipidemia were not significantly different between the 2 groups. [2]

DISCUSSION

In this study, we successfully generated a novel mouse model expressing DTR on renal fibroblasts and demonstrated that the administration of DT to healthy kidneys causes the upregulation of Ngal and the proliferation of tubular cells, whereas the administration of DT to fibrotic kidneys inhibits tubular proliferation. We further proposed that RA signaling might be one of the signaling pathways modified by DT administration, which has the potential to improve tubular regeneration. More importantly, we demonstrated the relocation of RALDH2 expression from proximal tubules to myofibroblasts during kidney injury and showed that this relocation is reversible after regeneration. The acquisition of RALDH2 expression by myofibroblasts also was observed in IgA nephropathy; the patients with RALDH2 staining in the interstitium were older and had lower kidney function. These results provide clear evidence of the beneficial role of fibrosis in the kidney, at least in the early phase, and provide insight into the long-lasting debate regarding the role of fibrosis in the progression of kidney disease.

In our previous work, we demonstrated that proximal tubule injury induces the transition from fibroblasts to myofibroblasts.[8] Together with the findings reported in this article, the evidence suggests that proximal tubules lose their RA-producing ability during injury and alternatively endow fibroblasts with RA-producing ability by inducing their transition to myofibroblasts, which might support the regeneration of tubular epithelial cells.

Resident fibroblasts are capable of producing various factors that act on other cell types and tissues in the body. Cortical fibroblasts, for example, possess Epo-producing ability in healthy kidneys,[31] although they lose this ability in the transition to myofibroblasts and acquire extracellular matrix-producing ability instead.[2] In aged kidneys, in contrast, resident fibroblasts acquire the ability to produce homeostatic chemokines such as CXCL13 and CCL19, attract lymphocytes, and initiate the formation of tertiary lymphoid tissues, causing sustained inflammation and retarding kidney regeneration.[32] The RA-producing ability reported in this article is a new role for the myofibroblasts, which might support the regeneration of injured tubules. Fibroblasts are highly plastic and can acquire various roles in response to their microenvironment, then influence the microenvironment with their newly acquired phenotypes. Further analysis of the plasticity and diversity of fibroblasts will provide us with important clues to understand the renal microenvironment in various types of kidney diseases.

In our experimental model, some fibroblasts survive after DT administration. Indeed, we did observe fibroblast-like cells in the interstitium by electron microscopy after the administration of DT (Supplementary Figure S5A). The length of the interval between DT administration and cell death is expected to vary between cell types depending on each type's protein synthesis requirements. In our previous work,[8] proximal tubules with DTR expression were severely injured 3 days after the administration of DT and thus appear to be highly dependent on protein synthesis. The major limitation of our experiment, in fact, is the lack of long-term experiments in the UUO model. We were only able to observe *P0-Cre:iDTR* mice within 3 days after DT administration, because these mice subsequently became sick, possibly as a result of dysfunction of *P0-Cre* lineage-labeled cells throughout the body. An analysis of long-term renal outcomes after the depletion of myofibroblasts is required to determine whether fibrosis is beneficial or detrimental in the progression of kidney diseases.

Recently, 2 other investigative groups have analyzed the consequences of pericyte depletion. In *FoxD1-Cre:iDTR* mice, Lemos *et al.*[33] observed acute kidney injury together with endothelial cell swelling and peritubular capillary loss 96 hours after the administration of DT. This severe phenotype of *FoxD1-Cre:iDTR* mice compared with our results might be

Figure 4 | Acquisition of retinoic acid (RA)–producing ability by myofibroblasts in various types of kidney disease models. (**a**) Immunostaining revealed strong retinaldehyde dehydrogenase 2 (RALDH2) expression in the interstitium in adenine nephropathy (AN) and severe ischemic reperfusion injury (IRI) that co-localized with platelet–derived growth factor receptor (PDGFR-β), a marker of fibroblasts and myofibroblasts. (**b**) Real-time reverse transcriptase–polymerase chain reaction (RT-PCR) analysis revealed the induction of *RALDH2* expression in these models ($n = 4$–5). One-way analysis of variance (ANOVA) with repeated measurements and Bonferroni *post hoc* tests. *$P < 0.05$. Western blot analysis also showed strong upregulation of RALDH2 expression both in AN and severe IRI models ($n = 4$). (**c**) Immunostaining of RALDH2, α-SMA, and Kim1 in reversible kidney disease models: reversible unilateral ureteral obstruction (rUUO), moderate IRI, and AN. Immunostaining of the kidneys at day 3 of rUUO, day 4 of moderate IRI, and day 3 of AN showed tubular injury and RALDH2 expression in myofibroblasts. The repaired kidneys also were examined 14 days after releasing the UUO clamps (rUUO Rday 14 [14 days after releasing the ligation of the ureter]), 45 days after moderate IRI (moderate IRI day 45), and 3 weeks after reverting from a diet containing adenine to a normal diet (AN R3 week). Immunostaining of the repaired kidneys showed the disappearance of RALDH2 and α-SMA expression in the interstitium and Kim1 expression in the tubular epithelial cells. (**d**) Real-time RT-PCR analysis revealed that *RALDH2* expression was markedly increased in diseased kidneys and significantly decreased to basal levels in repaired kidneys ($n = 4$–6). One-way ANOVA with repeated measurements and Bonferroni *post hoc* tests. GADPH, glyceraldehyde-3-phosphate dehydrogenase; NT, nontreated; PDGFR, platelet–derived growth factor receptor. *$P < 0.05$. Bars = 20 μm. To optimize viewing of this image, please see the online version of this article at www.kidney-international.org.

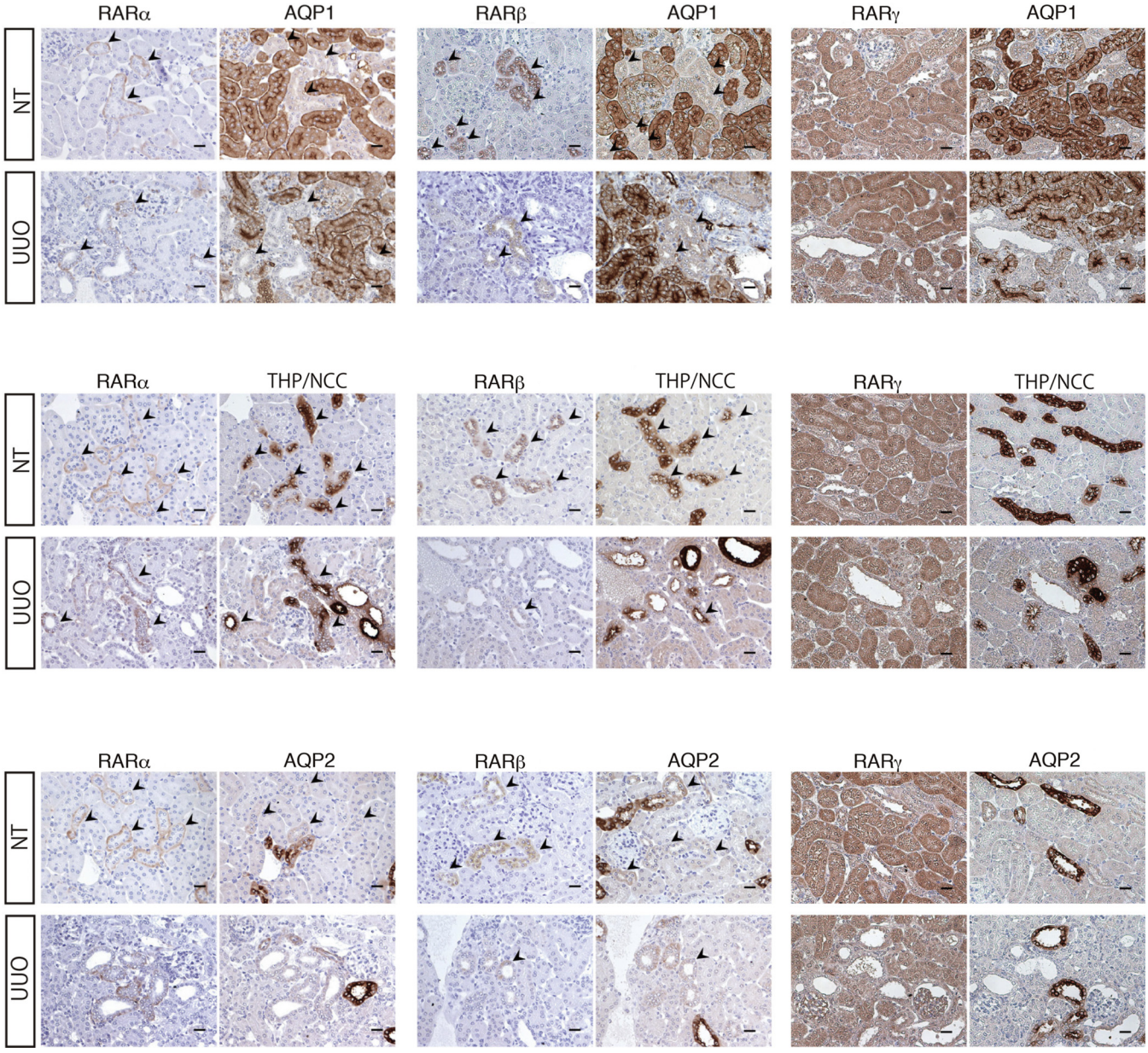

Figure 5 | Retinoic acid receptors (RARs) expressed in tubular epithelial cells. Immunohistochemical analysis of C57/BL6j mouse kidneys detected staining of RARs (RAR-α, -β and -γ) in tubular epithelial cells in both nontreated (NT) and unilateral ureteral obstruction (UUO) conditions. Whereas RARα and β were dominantly expressed in Tamm Horsfall protein (THP)/Na-Cl cotransporter (NCC)–positive distal tubules, RARγ was expressed in AQP1-positive proximal tubules in both NT and UUO kidneys. Arrowheads indicate the localization of RAR signals. Bars = 20 μm. To optimize viewing of this image, please see the online version of this article at www.kidney-international.org.

attributable to the recombination in different cell types. Whereas *FoxD1-Cre* causes recombination in all pericytes/fibroblasts in the kidney, *P0-Cre* causes recombination in fibroblasts in the cortex and outer medulla. Additionally, *FoxD1-Cre* causes recombination in vascular smooth muscle cells, mesangial cells, and podocytes.[34] Different recombination in pericytes/fibroblasts in the inner medulla and other cell types might contribute to the endothelial cell damage in *FoxD1-Cre:iDTR* mice, which, in turn, causes an abrupt increase in serum Cr. In *Gli1CreER^{t2}:iDTR* mice, Kramann *et al.*[35] showed endothelial cell damage and transient proximal tubule injury 10 days after DT administration and capillary loss 56 days after DT administration. In their article, the authors attributed the transient tubular injury to hypoxia as a consequence of capillary rarefaction. The timing of the analysis in this article is later than ours (day 3), which might contribute to the different behaviors in endothelial cells. Importantly, we observed proximal tubule injury without a significant reduction in endothelial cells (Supplementary Figure S1B) or capillary density (Supplementary Figure S5B) or turbulence in the capillary flow by live imaging (Supplemental Movie S1). The fact that we observed

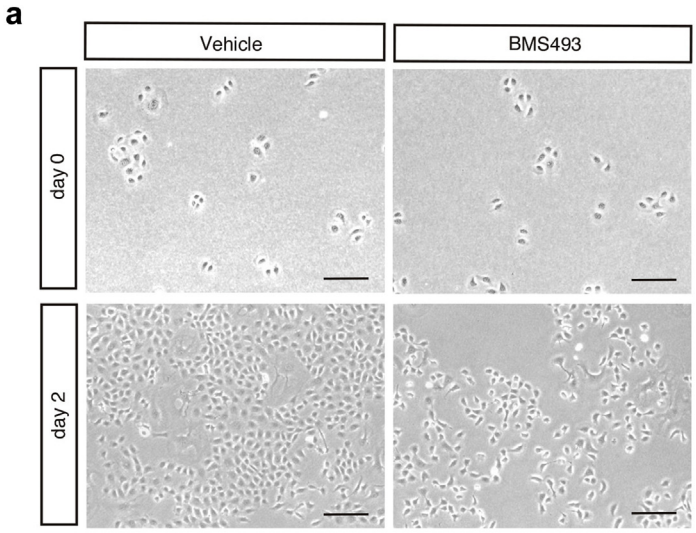
a
Vehicle
BMS493
day 0
day 2

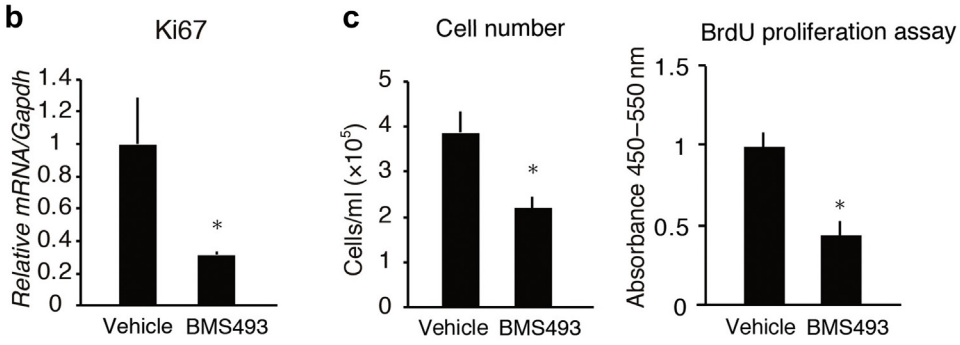
b
Ki67
Relative mRNA/Gapdh
1.4
1.2
1
0.8
0.6
0.4
0.2
0
*
Vehicle
BMS493
c
Cell number
Cells/ml (×10^5)
5
4
3
2
1
0
*
Vehicle
BMS493
BrdU proliferation assay
Absorbance 450–550 nm
1.5
1
0.5
0
*
Vehicle
BMS493

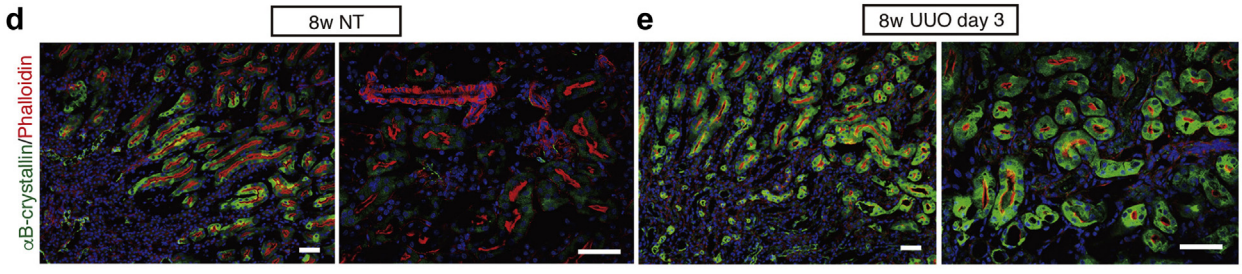
d
8w NT
αB-crystallin/Phalloidin
e
8w UUO day 3

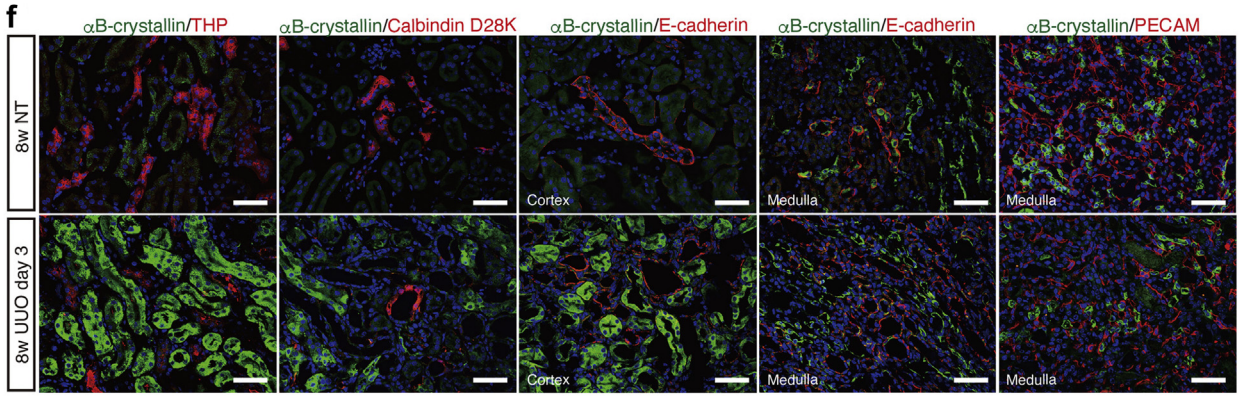
f
αB-crystallin/THP
αB-crystallin/Calbindin D28K
αB-crystallin/E-cadherin
αB-crystallin/E-cadherin
αB-crystallin/PECAM
8w NT
8w UUO day 3
Cortex
Medulla
Cortex
Medulla
Medulla

a

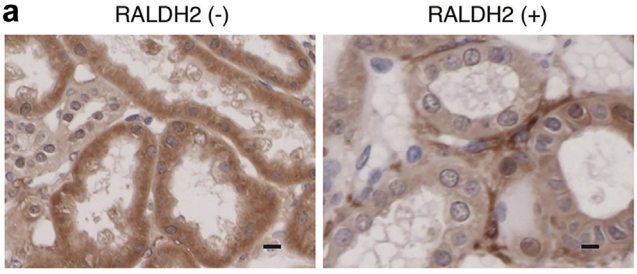

b

	RALDH2 (-) n = 15	RALDH2 (+) n = 12	*P* value
Age (years)	30 ± 3	48 ± 5	0.002
Male (%)	5 (33)	6 (50)	0.45
Cr (mg/dl)	0.7 ± 0.1	1.2 ± 0.2	0.008
eGFR ml/min per 1.73 m^2	100 ± 9	58 ± 7	0.002
BUN (mg/dl)	12 ± 1	18 ± 3	0.02
Urinary protein (g/day)	1.0 ± 0.2	1.8 ± 0.8	0.28
Hypertension (%)	1 (7)	3 (25)	0.18
Diabetes mellitus (%)	2 (13)	2 (17)	1
Dyslipidemia (%)	7 (47)	6 (50)	1

Figure 7 | Acquisition of retinaldehyde dehydrogenase 2 (RALDH2) expression by myofibroblasts in human kidney disease. (**a**) Representative images of the immunostaining of RALDH2 in biopsy samples from patients with IgA nephropathy. Whereas RALDH2 was mainly detected in tubular epithelial cells and was absent from the interstitium of the $RALDH2^-$ specimen (left), RALDH2-positive interstitial cells with a fibroblast-like morphology were detected in the interstitium of the $RALDH2^+$ specimen (right). (**b**) Characteristics of the study populations of IgA nephropathy with or without RALDH2 staining in the interstitium. Patients with positive RALDH2 staining in the interstitium were older and had lower kidney function. Other characteristics, including sex and risk factors such as hypertension, diabetes mellitus, and dyslipidemia, were comparable between the 2 groups. Percentages are shown in parentheses. BUN, blood urea nitrogen; eGFR, estimated glomerular filtration rate. Bars = 10 μm. To optimize viewing of this image, please see the online version of this article at www.kidney-international.org.

proximal tubule injury without obvious endothelial cell injury indicates a possible new role of fibroblasts in addition to the previously established cross talk between fibroblasts and endothelial cells. Together with the previous findings, our data suggest that fibroblasts/pericytes, proximal tubules, and peritubular capillaries are closely involved in mutual regulation in healthy and injured kidneys.

RA signaling plays an essential role in kidney development[36–39] and mediates the interaction between the ureteric bud and the stromal mesenchyme during kidney development.[40,41] RA secreted by stromal cells expressing RALDH2 controls Ret expression in the ureteric bud, which controls branching morphogenesis. Indeed, in human kidney development, the variants of *RALDH2* determine the final nephron number.[42] The observation that RA from stromal cells regulates the differentiation of epithelial cells is similar to our findings that RA from myofibroblasts possibly regulates tubular regeneration.

Recently, Chiba *et al.*[43] demonstrated that RA signaling in the proximal tubules represses proinflammatory macrophages and promotes renal regeneration after acute kidney injury. Whereas myofibroblasts expressed RALDH2 in the fibrosis model in our experiments, they showed that macrophages expressed RALDH2 in the acute kidney injury model. The source of RA might be variable depending on the type of kidney injury. More importantly, our research group and that of Chiba *et al.*[43] have independently demonstrated the importance of RA signaling during kidney injury and regeneration. In the healthy liver, retinols are taken up by hepatocytes and then transferred to fibroblast-like hepatic stellate cells, where they are stored as retinyl esters or metabolized into RA.[44] Previous reports have demonstrated that renal fibroblasts possess the capacity to store retinyl esters.[45] The upregulation of RALDH2 during the transition of fibroblasts to myofibroblasts as shown here implies the possibility that RA synthesis occurs in myofibroblasts.

In conclusion, fibroblasts acquire RA-producing capacity in the transition to myofibroblasts and may stimulate tubular regeneration. In our previous work, we proposed that fibrosis is secondary to tubular injury and that the treatment of fibrosis in its own right might be insufficient to halt the progression of kidney diseases.[8] The findings in this study further suggest the possible beneficial effect of fibrosis, at least in the early phase, but the long-term effect of fibrosis is still unknown. Further analysis is required to identify any molecular marker that could enable us to distinguish beneficial fibrosis from detrimental fibrosis.

CONCISE METHODS

Statistical analysis

Differences between the 2 groups were compared using the Student *t*-test for continuous variables and Fisher exact test for categorical variables as appropriate. Continuous variables were presented as mean ± SD, and categorical variables were expressed as number and percentage. Data in Figures 1e, 2e, 3d, 3e, 4b, and 4d were analyzed using a repeated measure 1-way or 2-way analysis of variance to obtain the Bonferroni adjusted *P* value and multiply the uncorrected *P* value by the total number of comparisons. All tests were 2-tailed,

Figure 6 | Possible retinoic acid (RA) signaling in proximal tubules. (**a**) Representative images of NRK52E in the presence or absence of BMS493. The numbers of NRK52E cells were apparently lower in the presence of BMS493. (**b,c**) Real-time reverse transcriptase–polymerase chain reaction (RT-PCR) analysis of Ki67 (**b**), the quantification analysis of total cell numbers, and BrdU proliferation assay (**c**) after the treatment with vehicle or BMS493. Statistical analysis by Student *t*-test. *$P < 0.01$. (**d–f**) Immunohistochemical analysis of nontreated (NT) and unilateral ureteral obstruction (UUO) kidneys. (**d,e**) Immunofluorescence of αB-crystallin, the product of a retinoic acid receptor (RAR) target gene, and phalloidin (a marker of proximal tubule) in the cortex and cortico-medullary junction. (**f**) Immunofluorescence of αB-crystallin and Tamm-Horsfall protein (THP) (a marker of thick ascending limb), calbindin D28K (a marker of distal convoluted tubule[7]), E-cadherin (a marker of distal convoluted tubule and collecting duct[7]), and platelet endothelial cell adhesion molecule (PECAM, a marker of endothelial cell). GADPH, glyceraldehyde-3-phosphate dehydrogenase. Bars = 200 μm (**a**), 50 μm (**d–f**). To optimize viewing of this image, please see the online version of this article at www.kidney-international.org.

and P values <0.05 or <0.01 were considered statistically significant. Student t-test and Fisher exact analyses were performed using JMP 13 software (SAS Institute, Cary, NC). One-way and 2-way analysis of variance analyses were performed using STATA software version 15 (StataCorp LLC, College Station, TX).

Detailed materials and methods are found in Supplementary Methods. Sequences of the primers used for real-time reverse transcriptase–polymerase chain reaction are listed in Supplementary Table S2.

ACKNOWLEDGMENTS

This research was supported by the Japan Agency for Medical Research and Development (AMED) under grant numbers JP18gm5010002 and JP18gm0610011; partially by KAKENHI Grant-in-Aids for Scientific Research B (17H04187), Grant-in-Aid for Scientific Research on Innovative Areas "Stem Cell Aging and Disease" (17H05642), and "Lipoquality" (18H04673) from the Japan Society for the Promotion of Science (JSPS); and grants from the Uehara Memorial Foundation, the Takeda Science Foundation, Yukiko Ishibashi Foundation, and the Sumitomo Foundation. Part of this work appeared as abstracts at the annual meetings of the American Society of Nephrology (November 11–16, 2014, Philadelphia, PA; November 5–10, 2013, Atlanta, GA; and October 30–November 4, 2012, San Diego, CA).

DISCLOSURE

JN was a graduate student when he conducted the experiments reported in this paper and was employed by Astellas after his graduation. SW is employed by Kyowa Hakko Kirin. JT is employed by Mitsubishi Tanabe Pharma. MY is on the advisory board of Astellas and J-DOPPS and receives research grants from Astellas, Chugai, Daiichi Sankyo, Fujiyakuhin, Kyowa Hakko Kirin, Mitsubishi Tanabe, MSD, Nippon Boehringer Ingelheim, and Torii.

All the other authors declared no competing interests.

SUPPLEMENTARY MATERIAL

Figure S1. Analysis of histologic injury and cell numbers in the interstitium of *P0-Cre:iDTR* mice after the administration of diphtheria toxin (DT). (**A**) Histologic analysis was performed in a section stained with periodic acid–Schiff. Histologic injury scores of nontreated kidneys in *P0-Cre:iDTR* mice were not significantly changed by the administration of DT except for sporadic vacuolation in proximal tubules. Histologic injury scores of unilateral ureteral obstruction (UUO) kidneys in *P0-Cre:iDTR* mice were not significantly changed by the administration of DT. (**B**) The number of white blood cells, endothelial cells, and fibroblasts in the interstitium 3 days after DT treatment. Control: control mice ($n = 4$); DT: DT-treated mice ($n = 5$). (**C**) Immunostaining of caspase-3 and γH2AX revealed that massive apoptosis was not observed in the proximal tubules of DT-treated kidneys. Right panels indicate massive apoptosis in the kidney with cisplatin-induced nephrotoxicity (CIN). Bar = 20 μm (**A**), 50 μm (**C**). Statistical analysis by Student t-test. n.s., not significant. $^*P < 0.01$.

Figure S2. Diphtheria toxin (DT) administration does not cause toxicity in mice that do not express DT receptor (DTR), but it causes the reduction of proximal tubule proliferation in *P0-Cre:iDTR* mice. (**A**) Real-time reverse transcriptase–polymerase chain reaction analysis revealed that *Ngal* mRNA was not significantly increased in *P0-Cre:iDTR(-)* mice kidneys after the administration of DT ($n = 4$-6). Histologic change in kidney sections stained with periodic acid–Schiff or the elevation of serum creatinine (Cr) and blood urea nitrogen (BUN) levels was not observed in *P0-Cre:iDTR(-)* mice after DT administration. (**B**) Graph illustrating the proportion of $Ki67^+$ cells in proximal tubules of unilateral ureteral obstruction (UUO) kidneys in *P0-Cre:iDTR* mice with or without DT administration ($n = 3$). Proximal tubule proliferation was significantly attenuated after DT administration. Bars = 20 μm. GADPH, glyceraldehyde-3-phosphate dehydrogenase; n.s., not significant. Statistical analysis by Student t-test: (**A**) $^*P < 0.05$; (**B**) $^*P < 0.01$.

Figure S3. Expression profiles of retinaldehyde dehydrogenases (RALDHs) in the kidney. (**A**) Graph illustrating the signal value of *RALDH1, RALDH2,* and *RALDH3* in sham and unilateral ureteral obstruction (UUO) kidneys from GeneChip analysis in the National Center for Biotechnology Information Gene Expression Omnibus database ($n = 3$). There were 3 probes for *RALDH3*. *RALDH2* expression was significantly upregulated in UUO kidneys, whereas *RALDH1* expression was comparable between healthy and UUO kidneys. *RALDH3* was almost completely absent from both healthy and UUO kidneys. (**B**) Real-time reverse transcriptase–polymerase chain reaction analysis confirmed that *RALDH1* expression was not increased in UUO kidneys ($n = 5$-8). *RALDH1* expression was increased after the administration of diphtheria toxin (DT) in both normal and UUO kidneys. (**C**) Immunostaining revealed that RALDH1 staining was detected in tubular epithelial cells but not in the interstitium. NT, nontreated. Bars = 50 μm. $^*P < 0.05$. Statistical analysis by Student t-test (**A, B**).

Figure S4. Histologic findings of reversible kidney disease models. Kidneys from 3 types of reversible kidney disease models, namely, reversible unilateral ureteral obstruction (rUUO), reversible moderate ischemic reperfusion injury (IRI), and reversible adenine nephropathy (AN), were analyzed in sections stained with periodic acid–Schiff. On day 3 of rUUO, day 4 of moderate IRI, and day 3 of AN, the treated kidneys showed tubular injury, whereas 14 days after releasing the UUO clamps (rUUO R day 14), 45 days after moderate IRI (moderate IRI day 45), and 3 weeks after reverting from an adenine-containing diet to a normal diet (AN R 3 weeks), this injury was almost completely repaired. Bars = 20 μm.

Figure S5. Existence of fibroblast-like cells in the interstitium and maintained expression of platelet endothelial cell adhesion molecule (PECAM) after the administration of diphtheria toxin (DT) in *P0-Cre:iDTR* mice. (**A**) Electron microscopy revealed the existence of fibroblast-like interstitial cells (arrowhead) after the administration of DT in *P0-Cre:iDTR* mice. **(B)** Immunostaining revealed that PECAM staining was not significantly decreased in DT-treated kidneys of *P0-Cre:iDTR* mice. Bars = (**A**) 2 μm, (**B**) 20 μm. The vessels in the DT-treated kidneys of *P0-Cre:iDTR* mice are also visualized in Supplementary Movie S1.

Movie S1A. *In vivo* multi-photon imaging of *P0-Cre:iDTR* mouse kidneys (**A**, control mice without diphtheria toxin [DT] injection; **B** and **C**, with DT injection). Tubules are visualized by the green autofluorescence signal. Texas-red bovine serum albumin was administered i.v. to label the cortical peritubular capillaries (PTCs). Capillary blood flow was confirmed by the shadows of circulating cells in PTCs. Capillary flow was maintained even after DT administration, and neither red blood cell rouleaux formation nor leakage from capillary to tubular lumen was detected (**B**). Very rarely, reduced PTC flow was observed around severely injured tubules (**C**). (**A**) Time series of PTC flow in the *P0-Cre:iDTR* mice without DT injection.

Movie S1B. Time series of PTC flow in the *P0-Cre:iDTR* mice with DT injection. Tubules in this image were almost intact.

Movie S1C. Time series of PTC flow in the *P0-Cre:iDTR* mice with DT injection. Injured tubules were observed in this image. Images were taken over 50 s. Scale = 50 μm.

Table S1. Result of Ingenuity Pathways Analysis.

Table S2. Sequences of primers used for real-time reverse transcriptase–polymerase chain reaction.

Supplementary Methods.

Supplementary material is linked to the online version of the paper at www.kidney-international.org.

REFERENCES

1. Kaissling B, Le Hir M. The renal cortical interstitium: morphological and functional aspects. *Histochem Cell Biol*. 2008;130:247–262.
2. Asada N, Takase M, Nakamura J, et al. Dysfunction of fibroblasts of extrarenal origin underlies renal fibrosis and renal anemia in mice. *J Clin Invest*. 2011;121:3981–3990.
3. Humphreys BD, Lin SL, Kobayashi A, et al. Fate tracing reveals the pericyte and not epithelial origin of myofibroblasts in kidney fibrosis. *Am J Pathol*. 2010;176:85–97.
4. Kramann R, DiRocco DP, Humphreys BD. Understanding the origin, activation and regulation of matrix-producing myofibroblasts for treatment of fibrotic disease. *J Pathol*. 2013;231:273–289.

5. Mack M, Yanagita M. Origin of myofibroblasts and cellular events triggering fibrosis. *Kidney Int*. 2015;87:297–307.
6. Duffield JS. Cellular and molecular mechanisms in kidney fibrosis. *J Clin Invest*. 2014;124:2299–2306.
7. Endo T, Nakamura J, Sato Y, et al. Exploring the origin and limitations of kidney regeneration. *J Pathol*. 2015;236:251–263.
8. Takaori K, Nakamura J, Yamamoto S, et al. Severity and frequency of proximal tubule injury determines renal prognosis. *J Am Soc Nephrol*. 2016;27:2393–2406.
9. Grgic I, Campanholle G, Bijol V, et al. Targeted proximal tubule injury triggers interstitial fibrosis and glomerulosclerosis. *Kidney Int*. 2012;82:172–183.
10. Fujigaki Y, Muranaka Y, Sun D, et al. Transient myofibroblast differentiation of interstitial fibroblastic cells relevant to tubular dilatation in uranyl acetate-induced acute renal failure in rats. *Virchows Arch*. 2005;446:164–176.
11. Kaissling B, Lehir M, Kriz W. Renal epithelial injury and fibrosis. *Biochim Biophys Acta*. 2013;1832:931–939.
12. Yamauchi Y, Abe K, Mantani A, et al. A novel transgenic technique that allows specific marking of the neural crest cell lineage in mice. *Dev Biol*. 1999;212:191–203.
13. Saito M, Iwawaki T, Taya C, et al. Diphtheria toxin receptor-mediated conditional and targeted cell ablation in transgenic mice. *Nat Biotechnol*. 2001;19:746–750.
14. Buch T, Heppner FL, Tertilt C, et al. A Cre-inducible diphtheria toxin receptor mediates cell lineage ablation after toxin administration. *Nat Methods*. 2005;2:419–426.
15. Honjo T, Nishizuka Y, Hayaishi O. Diphtheria toxin-dependent adenosine diphosphate ribosylation of aminoacyl transferase II and inhibition of protein synthesis. *J Biol Chem*. 1968;243:3553–3555.
16. Das BC, Thapa P, Karki R, et al. Retinoic acid signaling pathways in development and diseases. *Bioorg Med Chem*. 2014;22:673–683.
17. Kawaguchi R, Yu J, Honda J, et al. A membrane receptor for retinol binding protein mediates cellular uptake of vitamin A. *Science*. 2007;315:820–825.
18. Bouillet P, Sapin V, Chazaud C, et al.: Developmental expression pattern of Stra6, a retinoic acid-responsive gene encoding a new type of membrane protein. *Mech Dev*. 1997;63:173–186.
19. O'Byrne SM, Wongsiriroj N, Libien J, et al. Retinoid absorption and storage is impaired in mice lacking lecithin:retinol acyltransferase (LRAT). *J Biol Chem*. 2005;280:35647–35657.
20. Duester G, Mic FA, Molotkov A. Cytosolic retinoid dehydrogenases govern ubiquitous metabolism of retinol to retinaldehyde followed by tissue-specific metabolism to retinoic acid. *Chem Biol Interact*. 2003;143–144:201–210.
21. Gudas LJ. Emerging roles for retinoids in regeneration and differentiation in normal and disease states. *Biochim Biophys Acta*. 2012;1821:213–221.
22. Blomhoff R, Blomhoff HK. Overview of retinoid metabolism and function. *J Neurobiol*. 2006;66:606–630.
23. Wang Z, Famulski K, Lee J, et al. TIMP2 and TIMP3 have divergent roles in early renal tubulointerstitial injury. *Kidney Int*. 2014;85:82–93.
24. Grgic I, Krautzberger AM, Hofmeister A, et al. Translational profiles of medullary myofibroblasts during kidney fibrosis. *J Am Soc Nephrol*. 2014;25:1979–1990.
25. Ratnam KK, Feng X, Chuang PY, et al. Role of the retinoic acid receptor-alpha in HIV-associated nephropathy. *Kidney Int*. 2011;79:624–634.
26. Moreno-Manzano V, Mampaso F, Sepulveda-Munoz JC, et al. Retinoids as a potential treatment for experimental puromycin-induced nephrosis. *Br J Pharmacol*. 2003;139:823–831.
27. Wagner J, Dechow C, Morath C, et al. Retinoic acid reduces glomerular injury in a rat model of glomerular damage. *J Am Soc Nephrol*. 2000;11:1479–1487.
28. Lehrke I, Schaier M, Schade K, et al. Retinoid receptor-specific agonists alleviate experimental glomerulonephritis. *Am J Physiol Renal Physiol*. 2002;282:F741–F751.
29. Kishimoto K, Kinoshita K, Hino S, et al. Therapeutic effect of retinoic acid on unilateral ureteral obstruction model. *Nephron Exp Nephrol*. 2011;118:e69–e78.
30. Rhinn M, Dolle P. Retinoic acid signalling during development. *Development*. 2012;139:843–858.
31. Obara N, Suzuki N, Kim K, et al. Repression via the GATA box is essential for tissue-specific erythropoietin gene expression. *Blood*. 2008;111:5223–5232.
32. Sato Y, Mii A, Hamazaki Y, et al. Heterogeneous fibroblasts underlie age-dependent tertiary lymphoid tissues in the kidney. *JCI Insight*. 2016;1:e87680.
33. Lemos DR, Marsh G, Huang A, et al. Maintenance of vascular integrity by pericytes is essential for normal kidney function. *Am J Physiol Renal Physiol*. 2016;311:F1230–F1242.
34. Kobayashi A, Mugford JW, Krautzberger AM, et al. Identification of a multipotent self-renewing stromal progenitor population during mammalian kidney organogenesis. *Stem Cell Rep*. 2014;3:650–662.
35. Kramann R, Wongboonsin J, Chang-Panesso M, et al. Gli1+ pericyte loss induces capillary rarefaction and proximal tubular injury. *J Am Soc Nephrol*. 2017;28:776–784.
36. Burrow CR. Retinoids and renal development. *Exp Nephrol*. 2000;8:219–225.
37. Mendelsohn C, Lohnes D, Decimo D, et al. Function of the retinoic acid receptors (RARs) during development (II). Multiple abnormalities at various stages of organogenesis in RAR double mutants. *Development*. 1994;120:2749–2771.
38. Kastner P, Mark M, Ghyselinck N, et al. Genetic evidence that the retinoid signal is transduced by heterodimeric RXR/RAR functional units during mouse development. *Development*. 1997;124:313–326.
39. Bhat PV, Manolescu DC. Role of vitamin A in determining nephron mass and possible relationship to hypertension. *J Nutr*. 2008;138:1407–1410.
40. Batourina E, Gim S, Bello N, et al. Vitamin A controls epithelial/mesenchymal interactions through Ret expression. *Nat Genet*. 2001;27:74–78.
41. Mendelsohn C, Batourina E, Fung S, et al. Stromal cells mediate retinoid-dependent functions essential for renal development. *Development*. 1999;126:1139–1148.
42. El Kares R, Manolescu DC, Lakhal-Chaieb L, et al. A human ALDH1A2 gene variant is associated with increased newborn kidney size and serum retinoic acid. *Kidney Int*. 2010;78:96–102.
43. Chiba T, Skrypnyk NI, Skvarca LB, et al. Retinoic acid signaling coordinates macrophage-dependent injury and repair after AKI. *J Am Soc Nephrol*. 2016;27:495–508.
44. Lee YS, Jeong WI. Retinoic acids and hepatic stellate cells in liver disease. *J Gastroenterol Hepatol*. 2012;27(suppl 2):75–79.
45. Nagy NE, Holven KB, Roos N, et al. Storage of vitamin A in extrahepatic stellate cells in normal rats. *J Lipid Res*. 1997;38:645–658.